J. Phys.: Condens. Matter **20** (2008) 374121 (14pp) doi:10.1088/0953-8984/20/37/374121

Single-molecule transport in three-terminal devices

E A Osorio[1], T Bjørnholm[2], J-M Lehn[3], M Ruben[3,4] and H S J van der Zant[1]

[1] Kavli Institute of Nanoscience, Delft University of Technology, PO Box 5046, NL-2600GA, The Netherlands
[2] Nano-Science Center (Department of Chemistry and Niels Bohr Institute), University of Copenhagen, Universitetsparken 5, DK-2100 Copenhagen, Denmark
[3] ISIS/Université Louis Patseur, 8, Allée Gaspard Monge, BP 70028, F-67083 Strasbourg Cedex, France
[4] Forschungszentrum Karlsruhe GmbH, Institut für Nanotechnologie, Postfach 3640, D-76021 Karlsruhe, Germany

E-mail: h.s.j.vanderzant@tudelft.nl

Received 15 February 2008, in final form 11 May 2008
Published 26 August 2008
Online at stacks.iop.org/JPhysCM/20/374121

Abstract
Transport through single molecules has been studied using different test beds. In this paper we focus on three-terminal devices in which a molecule bridges the gap between two gold electrodes and a third electrode—the gate—is able to modulate the conduction properties of the junction. Depending on the electronic coupling, Γ, between the molecule and the gold electrodes, different transport regimes can be distinguished. We show measurements on junctions incorporating different single-molecule systems which demonstrate the distinction between these regimes, as well as the experimental limitations in controlling the exact value of Γ.

(Some figures in this article are in colour only in the electronic version)

1. Introduction

Transport through single molecules [1–5] is a field of intense investigation and, to date, several techniques are used to study transmolecular conduction, each with their advantages and disadvantages. For instance, scanning tunneling microscopy (STM) has proven to be a powerful tool for investigating inelastic electron tunneling spectroscopy (IETS) on single molecules [6–9]. STM offers imaging capabilities which allows spectroscopic studies in a well-defined experimental geometry. Single molecules in planar three-terminal devices, on the other hand, cannot be imaged easily. Moreover, the coupling to the leads and the molecular environment can differ from sample to sample (the same holds for two-terminal techniques such as mechanical break junctions). Nevertheless, the gate electrode in three-terminal devices—which is absent in STM and two-terminal techniques—allows studies in which the molecule can be oxidized or reduced; this makes it particularly interesting to study transmolecular conduction in different transport regimes. The third electrode can bring molecular levels into and out of resonance with the Fermi energy of the electrodes probing excited states and allowing different charge states to be accessed. Excited states can either be vibrational [10–12], electronic [13] or related to spin transitions [14, 15]. These excitations serve as a fingerprint of the molecule under study. Three-terminal devices are spectroscopic tools which allow the determination of addition energies in single-molecule junctions. Although it is possible to perform spectroscopy studies in two-terminal techniques [16], accurate estimates of the addition energies are hard to obtain if consecutive charge states cannot be probed.

The shift at which the orbital levels, E_n, can be moved up and down by the gate electrode potential, V_G, is quantified by the gate coupling parameter β. In an experiment, it should be as large as possible in order to access as many charge states as possible. The geometry plays an important role in the gate coupling and one should take care that the electrodes themselves do not screen the gate potential as this would decrease β. The electrode separation (and therefore the length of the molecule) and the breakthrough voltage of the gate

oxide are other important parameters. Currently, two gate materials are frequently used: heavily doped silicon substrates with thermally grown SiO_2 on top and aluminum strips with a native Al_2O_3 oxide of only a few nanometers. For aluminum gates with an oxide thickness of 3 nm, the gate coupling is about 0.1 so that, with a typical breakthrough voltage of 4 V at low temperatures, the potential of the molecular levels can be shifted by ± 0.4 eV. On the other hand in silicon devices with an SiO_2 thickness of 250 nm, the gate coupling is about 10^{-3}; with a typical breakthrough voltage of 100 V, the range over which the potential on the molecule can be varied equals ± 0.1 eV.

This paper starts with a brief description of the different approaches that have been used to fabricate three-terminal devices (section 2). Following this, we will discuss the different transport regimes, and mechanisms for conduction through molecular quantum dots (section 3). In section 4, we detail our fabrication method, the molecule-junction preparation and the measurement techniques. Next we present experimental results which exemplify the different transport regimes discussed in section 3. We end with a brief summary and outlook in section 6.

2. Three-terminal devices

Three-terminal devices have been fabricated using different techniques. They notably differ in the way the nanogap or the molecular junction is created. We use the electromigration technique, in which a large current density breaks a narrow and thin metal wire to form two physically separated electrodes [17]. Electromigration-induced nanogap formation has been imaged *in situ* by transmission (and scanning) electron microscopy [18, 19]. Several of these electrode pairs can be fabricated on top of a conducting substrate (coated by an insulating layer) which can then serve as a gate electrode. Although some control has been obtained over the electromigration process by using a feedback mechanism, the resulting nanogap geometry or size remains uncontrollable. The advantage of electromigrated devices on a Al/Al_2O_3 gate electrode is their large gate coupling ($\beta_{MAX} \sim 0.27$). The planar geometry (see figure 2.1(a)) offers a large stability for systematic studies as a function of gate voltage, temperature and magnetic field as we will show in section 5. Molecules are deposited from solution either prior to gap formation or afterward.

A second technique involves the fabrication—on top of a gate electrode—of two gold electrodes using a shadow mask technique as illustrated in figure 2.1(b). If the tilt angle of evaporation is high there is no overlap between the source and drain shadows. Reducing the tilt angle decreases the source–drain gap. *In situ* measurements of the conductance allows for fine tuning of the gap distance when performed at low temperatures (~4.2 K). Molecules are deposited by quench condensation without disruption of the vacuum [20, 21]. The advantages of this evaporation technique include all the ones from the electromigrated devices, plus the control over the gap distance and the ability for molecule deposition inside a clean

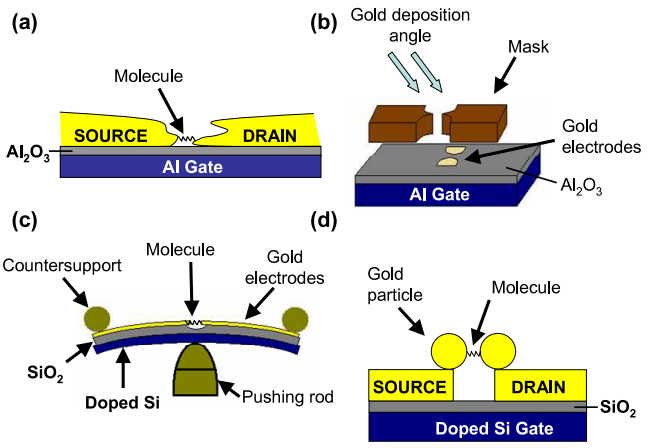

Figure 2.1. Schematic diagrams of different three-terminal device techniques. (a) Electromigrated thin metal wire on top of a Al/Al_2O_3 gate electrode. (b) Angle evaporation technique to fabricate planar electrodes with nanometer separation on top of a Al/Al_2O_3 gate electrode. (c) Gated mechanical break junction. (d) The dimer contacting scheme (see text).

environment. Typical gate coupling values are of the same order as the ones for electromigrated junctions.

Only recently it has been possible to integrate a gate electrode in mechanical controllable break junctions (MCBJ) [22]. In a MCBJ, suspended metallic wires with predefined breaking points are patterned on top of a bendable substrate (see figure 2.1(c)). By bending the substrate in a three-point support, the metallic wire can be broken in two electrodes; the gap distance can then be tuned with picometer resolution. So far it has been possible to place the gate electrode from the gap at a distance of 40 nm [22]. Although the gate coupling remains low as compared to other techniques with a planar geometry ($\beta \sim 0.006$ in [22]), MCBJ have the clear advantage of precise control over the gap distance; the reported breakthrough voltage [22] was 12 V. Molecule deposition is carried out from solution.

Another three-terminal approach was recently reported by Dadosh *et al* [23]. Their method is based on synthesizing in solution a dimer structure consisting of two colloidal gold particles connected by a dithiolated molecule. The dimer is then electrostatically trapped between two gold electrodes defined on top of a gate electrode (see figure 2.1(d)). According to the authors, this dimer-based contacting scheme provides several advantages such as the ability to fabricate single-molecule devices with high certainty in which the contacts to the molecule are well defined. The gold particles in this set-up, however, efficiently screen the gate potential. Moreover at low temperatures, spectroscopic features of the gold particles were sometimes observed to be superimposed on the characteristics of the molecule conduction.

3. Transport through molecular junctions

In describing three-terminal transport through molecular junctions at cryogenic temperatures, the molecule is viewed as a confined electronic system—or quantum dot—coupled

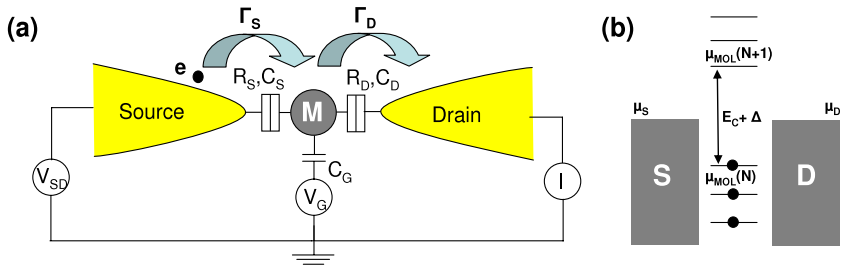

Figure 3.1. Schematic picture and energetics of a molecular quantum dot. (a) The molecular quantum dot (represented by a disk 'M') is connected to source and drain contacts via tunnel barriers, allowing charge carriers to tunnel to and from the quantum dot. The current through the device, I, is measured in response to a bias voltage, V_{SD}, and a gate voltage, V_G. (b) Electrochemical potentials—μ_{MOL}—for different electron numbers, with $\Delta(N) =$ level the spacing and $E_c =$ charging the energy.

by tunneling barriers to source and drain electrodes as schematically shown in figure 3.1(a) [24–27]. The discrete electronic spectrum of such an object is illustrated in figure 3.1(b); available states for transport are denoted by the electrochemical potential $\mu_{MOL}(N)$, which by definition is the minimum energy for adding the Nth electron to the dot: $\mu_{MOL}(N) = U(N) - U(N-1)$, where $U(N)$ is the total ground state energy for N electrons on the dot. The energy to add an extra electron or addition energy, E_{add}, equals the level spacing, $\Delta(N)$, plus the charging energy, E_C (see figure 3.1(b)). The latter quantity accounts for the Coulomb interactions between electrons in the dot and is defined as $E_C = e^2/C$. Here, C is the total capacitance to the 'outside world', i.e. $C = C_S + C_D + C_G$, where C_S is the capacitance to the source, C_D to the drain and C_G the capacitance to the gate. The overlap of the molecular wavefunction with that of the conduction electrons of the leads is described by the molecule–lead couplings Γ_S, Γ_D, which can also be related to the bare tunneling rates between the molecular level and each of the leads. The total coupling, $\Gamma = \Gamma_S + \Gamma_D$, is a measure of the resulting broadening of the molecular levels. In principle Γ can be charge-state-dependent as the overlap between the wavefunctions of the metal electrodes and the molecule can vary strongly with N (i.e. $\Gamma = \Gamma(N)$).

At cryogenic temperatures, $E_C, \Delta \gg k_B T$ (thermal energy). Depending on the value of Γ with respect to these parameters, we can distinguish two regimes of special interest. We will briefly discuss both in the next two sections.

3.1. Weak coupling regime

When Γ is very small ($\Gamma \ll E_C, \Delta$), one enters the weak coupling limit. Figure 3.2(a) schematically illustrates the result of a typical transport measurement in the form of a so-called stability diagram. Slanted lines separate regions of high conductance (single-electron tunneling (SET) regime, gray regions) from enclosed diamond-shaped regions (Coulomb diamonds) with almost[5] zero conductance (black regions). Inside the SET regime, lines running parallel to the diamond edges correspond to the onset at which excited states start contributing to the conductance; their energy, ΔE, can be read off as the distance from the zero-bias axis to the crossing point

[5] In first order, the conductance is zero. Higher-order processes, however, lead to a finite current in this regime, which is negligibly small if Γ is small.

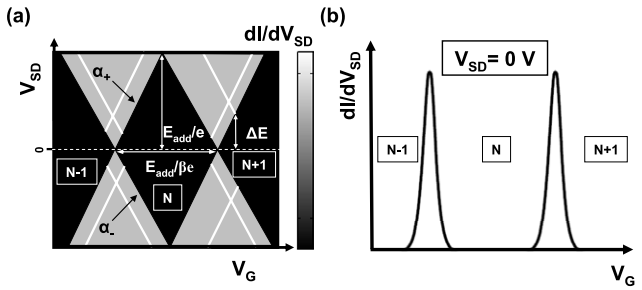

Figure 3.2. Electron transport through a weakly coupled molecular quantum dot; the gate voltage probes three different charge states. (a) Conductance map of the differential conductance, dI/dV_{SD}, versus V_{SD} and V_G (stability diagram). The edges of the diamond-shaped regions (black) correspond to the onset of current (gray). Diagonal lines emanating from the diamonds (white) indicate the onset of transport through excited states. (b) Coulomb peaks in differential conductance, dI/dV_{SD}, versus gate voltage in the linear-response regime (small bias voltage).

with the diamond edge as illustrated in figure 3.2(a). Inside the black diamond-shaped regions the number of electrons on the molecule is fixed to an integer value. Between consecutive black regions (charge states) the charge on the molecule increases (decreases) by one unit as we go to more positive (negative) gate voltages. It should be noted that it is difficult to assign a particular charge state of the free molecule to these states. For instance, the charge state measured at zero bias and zero-gate voltage may not be the neutral charge state of the molecule. At zero bias, partial charging of the molecule can take place in order to equilibrate the chemical potentials across the junction. Background charges from electron traps in the vicinity of the device may also introduce an offset in the level positions of the molecular quantum dot.

Resonant tunneling, which is a first-order process, lifts the Coulomb blockade. This occurs when a charge state, $\mu_{MOL}(N)$, lies in between the voltage-bias window defined by μ_S and μ_D. This can be done by independently sweeping the bias or gate voltage 'towards' the gray regions where current starts flowing by a sequential tunneling process (charges are taken from the source to the molecule and subsequently from the molecule to the drain). Sweeping the gate voltage and measuring the differential conductance at low bias results in a series of peaks as shown in figure 3.2(b). Each of these peaks

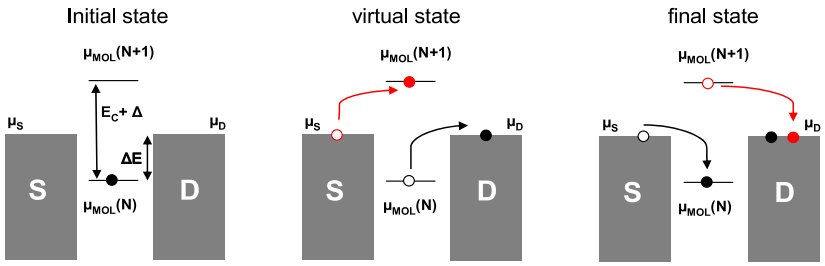

Figure 3.3. Elastic cotunneling. The Nth electron on the dot jumps to the drain (virtual state) to be immediately replaced (final state) by an electron from the source (black arrow sequence). A similar process involves the unoccupied state (red arrow sequence). In both examples, an electron is effectively transported from source to drain.

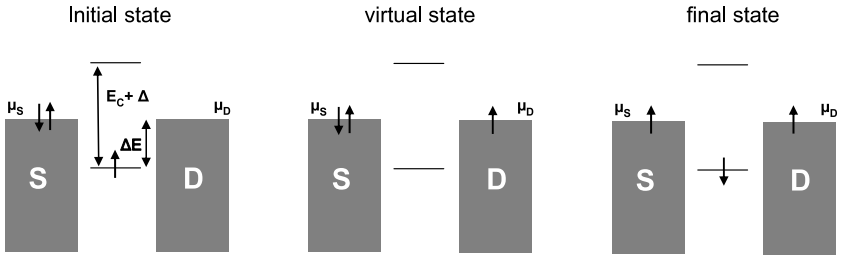

Figure 3.4. Spin-flip cotunneling. A spin-up electron jumps out of the dot (virtual state) to be immediately replaced by a spin-down electron (final state).

represents a charge degeneracy point or Coulomb oscillation. At these points, the two charge states $N(N-1)$ and $N+1(N)$ of the quantum dot have the same energy and hence an electron can hop on and off the dot freely.

The slopes of the diamond boundaries in figure 3.2(a) give quantitative information on the capacitances. Along the line with positive slope, $\alpha_+ = C_G/(C_G + C_D)$, the electrochemical potential level is aligned with the source and along the line with negative slope, $\alpha_- = -C_G/C_S$, it is aligned with the drain. The maximum extent of the diamond in $V_{SD}(V_G)$ is $E_{add}(E_{add}/\beta e)$ as illustrated in figure 3.2(a). The gate coupling defined as $\beta = C_G/C_\Sigma$ can either be determined from the diamond slopes ($\beta = \alpha_+\alpha_-/(\alpha_+ + \alpha_-)$) or by measuring the sizes of the diamond. From the conductance *map* it is also possible to determine the molecule–lead coupling Γ. One way of doing this is to evaluate the full width at half-maximum (FWHM) of the conductance peak along a diamond edge from the dI/dV_{SD} versus V_{SD} trace. In a similar way, the FWHM of the Coulomb peak (figure 3.2(b)) multiplied by β is a measure of Γ.

3.2. Intermediate coupling: cotunneling and Kondo effect

Higher-order tunneling [28] processes become more apparent when the tunnel coupling, Γ, is enhanced. In the so-called strong coupling regime ($\Gamma \gg E_C, \Delta(N), k_BT$) the electronic states on the dot and electrode are significantly hybridized, elastic coherent tunneling dominates transport and signatures of the Coulomb blockade are washed out by quantum fluctuations of the molecular charge; the resistance is close to the resistance quantum $R_Q = h/e^2 = 25.8\ \text{k}\Omega$. Between the weak coupling and strong coupling regimes we identify a third regime which we will refer to as the intermediate coupling regime. In this regime it is still possible to observe Coulomb diamonds, but higher-order processes lead to a non-negligible current inside the blockade regions. In this section we will discuss three different types of higher-order tunneling processes: elastic cotunneling, the Kondo effect, which is a particular elastic many-body effect, and inelastic cotunneling.

Figure 3.3 illustrates an elastic cotunneling process. Energy conservation forbids the number of electrons to change as this would cost an energy ΔE. Nevertheless, an electron can tunnel off the molecule, leaving it temporarily in a classically forbidden 'virtual state' (middle diagram in figure 3.3). By virtue of Heisenberg's energy–time uncertainty principle this is allowed as long as another electron tunnels into the molecule in the same quantum process in order not to violate energy conservation. The final state then has the same energy as the initial one, but one electron has been transported through the molecule. This elastic cotunneling process is analogous to the superexchange mechanism in chemical electron transfer theory [29, 30]. It occurs at arbitrarily low bias as the energy of the tunneling electron and the molecule are unchanged and leads to a nonzero background conductance in the blockade regions.

If the electron spin is taken into account, one can encounter another elastic cotunneling process connected to the Kondo effect [31–39]. Whenever a single localized state in the molecule is spin-degenerate and partially filled, the molecule has a net spin (magnetic moment). This, for example, occurs for an odd occupancy in the molecule (one electron is unpaired, $S = 1/2$). We shall consider this simple case. The conduction mechanism for the Kondo effect involves spin-flip events such as the one illustrated in figure 3.4. We refer to other papers [40–45] for a more detailed theoretical discussion.

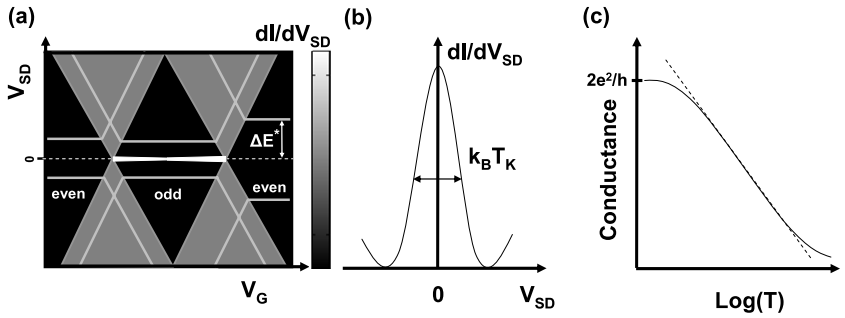

Figure 3.5. Schematic representation of the main characteristics of the Kondo effect in electron transport through a molecular quantum dot. (a) In the stability diagram, the Kondo effect results in a zero-bias resonance (white line) for an odd number of electrons in the dot. Inelastic cotunneling excitations appear as lines running parallel to the gate axis at finite bias. (b) For $T \ll T_K$, the full width at half-maximum (FWHM) of the Kondo resonance is $\sim k_B T_K$. (c) Temperature dependence of the Kondo-peak height in the middle of the Coulomb diamond.

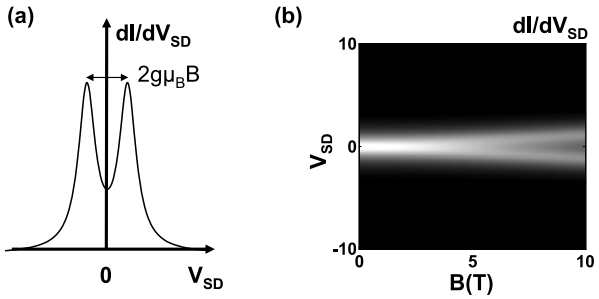

Figure 3.6. Characteristics of the Kondo effect in the presence of a magnetic field. (a) Zeeman splitting of the Kondo resonance at finite magnetic field. (b) Calculated grayscale plot of $\mathrm{d}I/\mathrm{d}V_{SD}$ versus V_{SD} and B.

Here, we concentrate on its main transport characteristics, which are summarized in figures 3.5 and 3.6.

For an odd number of electrons the stability plot shows a zero-bias resonance in the differential conductance, $\mathrm{d}I/\mathrm{d}V_{SD}$, versus V_{SD}, inside the Coulomb diamond 'connecting' both degeneracy points as shown in figure 3.5(a). For an even number of electrons with all spins paired, $S = 0$ and there is no Kondo resonance. This even–odd asymmetry is very helpful in assigning the parity of the charge state which can then add extra information to the understanding of the spectroscopic features observed in the stability plots. In the low temperature limit ($T \ll T_K$), the full width at half-maximum (FWHM) of the Kondo resonance is of the order of $k_B T_K$ (see figure 3.5(b)). Typical Kondo temperatures are $T_K \sim 1$ K for semiconductor quantum dots [34], $T_K \sim 1$–10 K for carbon nanotubes [46, 47] and $T_K \sim 20$–50 K for molecular devices [36–39]. In the middle of the Coulomb diamond, the height of the Kondo peak as a function of temperature is expected to show the characteristic form [33, 34]

$$G(T) = G_c + G_a(1 + 2^{(1/s)-1}T^2/T_K^2)^{-s} \qquad (1)$$

where G_a is the maximum conductance, G_c is a temperature-independent offset and $s = 0.22$ for $S = 1/2$. This dependence is drawn in figure 3.5(c) and the characteristic features include a conductance that increases logarithmically with decreasing temperature and saturates at a value $2e^2/h$ at the lowest temperatures in the case of symmetric lead–dot coupling. The latter is commonly referred to as Kondo in the unitary limit [48].

In a magnetic field the Zeeman splitting of the Kondo resonance leads to the observation of two Kondo peaks symmetric in bias, separated by twice the Zeeman energy as schematically illustrated in figure 3.6(a). Its evolution in a magnetic field is shown in figure 3.6(b). Although we have been only considering $S = 1/2$, it is important to note that other types of Kondo systems are possible owing to orbital degeneracies [49] or triplet states [50–52]; these can lead to a violation of the parity effect.

A cotunneling event that leaves the molecule in an excited state is called inelastic. An example of such a process is depicted in figure 3.7; as shown, the onset of the cotunneling event occurs at $eV_{SD} = \Delta E^*$, the condition dictated by the energy conservation principle. In transport measurements, inelastic cotunneling appears in the stability diagram inside the Coulomb diamonds as two symmetric lines running parallel to the gate axis as represented by the gray lines in figure 3.5(a); their energy, ΔE^*, is the distance of the excitation to the zero-bias axis as illustrated in figure 3.5(a). Furthermore the inelastic cotunneling line is expected to intersect, at the diamond boundary, the corresponding excitation line inside the SET region [53].

As a final remark, we note that higher-order coherent processes appear as sharp spectroscopic features as the conductance of the ith order process is proportional to Γ_i. For first-order incoherent single-electron tunneling, the current is proportional to Γ.

3.3. Vibrational effects

Molecules are 'flexible' objects, and can, for instance, undergo conformational changes that can strongly affect transport behavior [54–56]; vibrational modes lie typically between a few meV to tens of hundreds of meV for free molecules. Inelastic effects in molecular junctions originate from coupling between electronic and nuclear degrees of freedom [57–62]. The nuclei are much heavier than the electrons. Therefore the nuclear and electronic dynamics can be separated as is usually done in the Born–Oppenheimer approximation. The

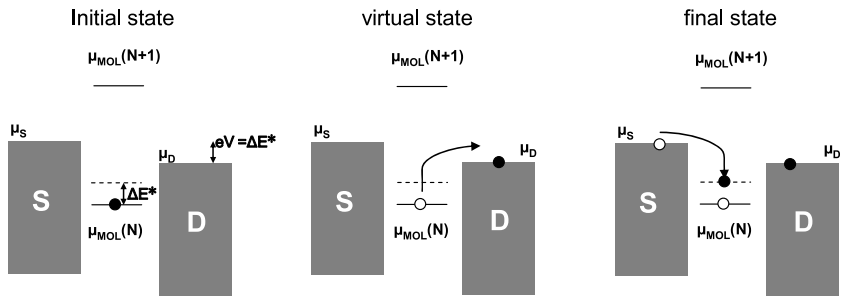

Figure 3.7. Inelastic cotunneling. For $eV_{SD} \geqslant \Delta E^*$, the Nth electron on the dot may jump from the ground state to the drain (virtual state) to be immediately replaced by an electron from the source (final state), which enters the excited state.

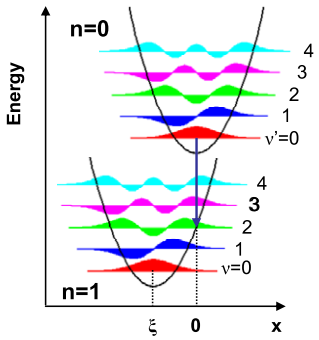

Figure 3.8. Franck–Condon principle. The schematic plot shows vibrational states and their wavefunctions of the neutral ($n = 0$, top) and charged molecule ($n = 1$, bottom). Electronic transitions are fast compared to changes in nuclear coordinates (x). Hence, transitions between vibrational states are vertical (blue arrow) and the corresponding matrix elements are given by the wavefunction overlap.

nuclear motion can be described by a series of uncoupled harmonic oscillators and for simplicity we consider one single vibrational mode. When an electron tunnels onto the molecule, the minimum of the nuclear (harmonic) potential is shifted from $x = 0$ to ξ (new equilibrium position) as illustrated in figure 3.8. This shift is induced by the new electronic configuration in the molecule. The displacement is described by the parameter λ which is the electron–phonon coupling. It is the ratio of the displacement and the quantum mechanical uncertainty, x_0, of the position in the vibrational ground state: $\lambda = \xi/x_0$.

Excitation of a molecular vibration is governed by the Franck–Condon principle (figure 3.8): assuming that initially the (neutral) molecule was in its ground vibrational state, the probability that the molecule ends in a particular vibrational level of the charged molecule is proportional to the square of the overlap integral between the vibrational wavefunctions of the initial, ψ_i, and final state, ψ_f; the last quantity is commonly referred to as the Franck–Condon factor [63]. As a consequence, the tunnel rates are modified to $\Gamma \rightarrow \Gamma_{elec}|\langle\Psi_f|\Psi_i\rangle|^2$. Note that, when there are no vibrational degrees of freedom, the overlap is one and the coupling Γ remains purely electronic. Once the electron hops off, the molecule can be left in a vibrational excited state (the vibrational energy being provided by the outgoing electron). In the sequential tunneling process described before, vibrational states of the charged molecule serve as additional resonance levels; the intensity of the excitation line inside the SET region is then determined by the corresponding Franck–Condon factors. The observation of multiple excitations lines with equal spacing may result from the excitation of an integer number of vibrational quanta as was first presented by Park *et al* [12] in C_{60} three-terminal molecular junctions. This is only possible for sufficient electron–phonon coupling and, in the work of Park, λ was estimated to be around one.

4. Nanogap fabrication, molecule-junction preparation and measurement techniques

4.1. Three-terminal device fabrication

Three-terminal devices are made using standard electron-beam lithography. In short, four steps are needed (see figure 4.1(a)). In the first step, contact pads and alignment markers are defined by evaporation of 3 nm Ti, 35 nm Au and 15 nm AuPd on top of an oxidized Si substrate. Secondly, the gate is defined by evaporating 75 nm Al. Subsequent exposure to O_2 for 15 min at 50 mTorr allows the formation of a 2–4 nm thick aluminum oxide layer. The third step involves the fabrication of a narrow (100 nm) and thin (12 nm) gold wire—without an adhesion sublayer—on top of the aluminum gate. In a final step, the thin gold wire is connected to the coarse pads by evaporation of 110 nm of AuPd. Figure 4.1(b) shows a SEM picture of a completed device.

4.2. Electromigration and gap fabrication

For the creation of a nanometer-sized gap suitable for contacting single molecules we first narrow the thin gold wire by electromigration to a few-atom constriction. The instability of these gold nanoconstrictions at room temperature—due to mobility and stress in the material—allows spontaneous breaking of the wire, resulting in two separate electrodes [64, 65]. On a timescale of tens of minutes or hours the wires break until they reach conductance values $\ll 100\ \mu$S without any applied bias. The uncontrolled nature of the 'self-breaking' process produces nanogaps in a range of sizes.

Electromigration is performed using an active breaking scheme, similar to the ones previously reported [66]. In the

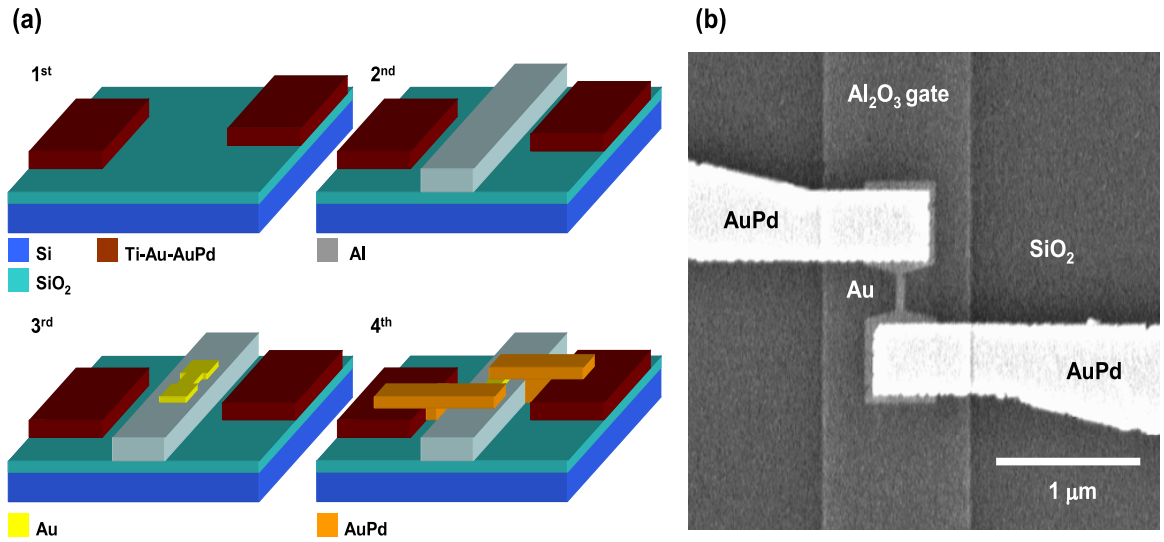

Figure 4.1. Three-terminal device fabrication. (a) Schematic overview of the four electron-beam lithography steps. (b) SEM image of a completed device prior to breaking.

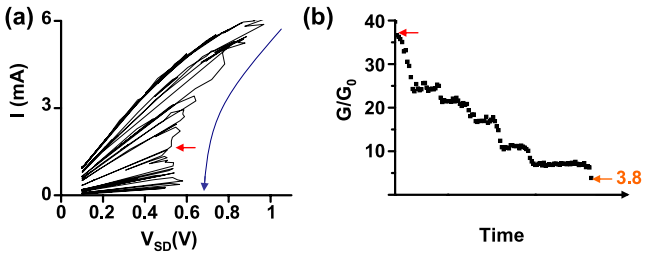

Figure 4.2. Electromigration with an active breaking scheme. (a) I–V_{SD} data from a succession of ramps across a junction. The blue arrow indicates its evolution as the nanoconstriction forms. (b) Same data truncated at the red arrow position in (a), with conductance (normalized by $G_0 = 2e^2/h$) versus data point. The final conductance is $3.8G_0 \approx 3.4$ kΩ.

active breaking process, the voltage is increased from below the electromigration threshold (∼200 mV) while sampling the current. If the absolute resistance of the wire increases by a value determined during the sweep, typically around 10%, the applied voltage is reduced back to 100 mV and the sweep is repeated with a new value for the wire resistance. A typical example of this process is shown in figure 4.2. With this method, nanoconstrictions with a resistance in the kΩ range can be achieved with high reproducibility.

4.3. Molecule–junction preparation and characterization

For the deposition of a molecule in the junction we use a home-made liquid cell, placed inside a ^{4}He cryostat, containing a 1 mM molecule solution. At room temperature, electromigration is performed in a liquid environment on about 16 junctions which are rinsed with the pure solvent, dried and cleaned in an oxygen plasma beforehand. Nanoconstrictions with a resistance in the kΩ range are first prepared as described above in the solution containing the molecules. The electromigrated junctions are then left in the molecule solution for about 1 h to allow for molecular self-assembly (if appropriate binding groups are used) and 'self-breaking' of the constricted gold wire. Junctions which did not 'self-break' within this time are then intentionally broken at conductances higher than G_0. Last, the sample space is evacuated and the cooling procedure to 1.7 K starts. This molecule deposition technique is similar to the one reported by Riel and coworkers in mechanical break junctions [67]. During electromigration, the junction temperature can reach a few hundred Kelvin [68]; performing the self-breaking in solution avoids excessive temperatures on the molecules and allows immediate exposure of the freshly created gap to the molecule solution. We should emphasize that sample contamination could still be an issue since preparation of the molecular junctions is not carried out under ultraclean high-vacuum conditions; layers of water or hydrocarbon molecules may then be present at the contact interface.

Once at base temperature, we characterize our junctions by measuring the current at a source–drain voltage in the range of 10–100 mV as a function of gate voltage from −3 to 3 V; above these voltages, gate leakage usually starts to set in. The gate traces can be categorized in four different ways, and typical examples are shown in figure 4.3.

- No current within the measurement accuracy (<10 pA for $V_{SD} = 50$ mV), indicating that the gap distance is a few nanometers or larger (figure 4.3(a)).
- Very weak, linear dependence on gate voltage (figure 4.3(b)) with less than a few per cent change in the current, the origin of which is not understood.
- Nonlinear, monotonic increase/decrease of the current (figure 4.3(c)).
- Traces showing one or more Coulomb peaks (figure 4.3(d)).

The traces in the two last categories may be a result of transmolecular conduction. Stability diagrams are recorded for all these devices. The differential conductance, dI/dV_{SD}, is

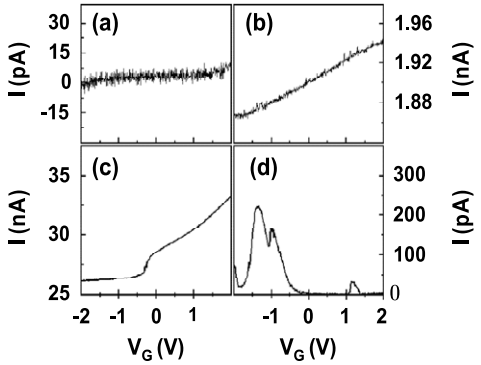

Figure 4.3. Junction characterization. The current as a function of gate voltage in the range of −2 to 2 V, measured at a bias voltage of 50 mV. (a)–(d) illustrate the different behaviors as discussed in the main text.

either measured directly, with a lock-in technique or obtained from numerical derivation of the I–V_{SD} characteristics. The stability diagrams of samples that exhibited nonlinear monotonic traces usually show the presence of one partial Coulomb diamond with a weak gate coupling ($\beta < 0.05$) and large addition energies >200 meV (figure 4.4(a)). It is difficult to make conclusive statements about these junctions since it is known that electromigration may lead to the formation of small gold clusters [69] which also may exhibit signatures of Coulomb blockade and the Kondo effect [35]. These junctions may then contain a molecule that is well shielded from the gate by the leads, or a gold grain that is well coupled to one of the electrodes (figure 4.4(a)). Samples that exhibit several Coulomb peaks (more than five) and addition energies smaller than 100 meV are unambiguously treated as junctions containing gold grains in direct contact with the gate dielectric. We find that these junctions show a high gate coupling ($\beta \sim 0.27$; see figures 4.4(b) and (c)). Furthermore it is very unlikely for a molecule to show more than five charge states with almost constant addition energies as this would mean that for such a small object the electronic spectrum remains unchanged upon the addition of extra charges (figure 4.4(b)). We note that, when using the self-breaking scheme, multiple Coulomb diamonds with high gate coupling are not observed; figures 4.4(b) and (c) are from junctions that were actively broken into high conductances (no self-breaking).

At this point the remaining question is what are the characteristic features for transport through single molecules. Electron addition energies for molecules are expected to be larger than 100 meV. In addition, transport that is due to single molecules has consistently shown (see the next section) a gate coupling that does not exceed 0.15, which can be explained by the fact that molecules are elevated from the gate oxide when connected to gold. Last, we look at generic features present in measurements carried out on the same molecule, such as addition energies, electronic excitation energies and vibrational excitations. This can only be done if a large ensemble of samples has been measured. Furthermore, stability diagrams may contain subtle information about the presence of molecules. For example, one may expect the gate and electronic couplings to be largely charge-dependent because the charge density may differ from orbital to orbital. For gold grains, where the interaction is dominated by the Coulomb repulsion of the electrons (classical dot regime, see figure 4.4(b)) the smallness of the quantum splitting indicates that the charge distribution of successive orbitals is very similar. Hence we do not expect strong variations of the couplings in that case.

5. Transport regimes revealed in experiments

In the experiment we are not able to control Γ for any molecule we have studied so far. Consequently some junctions may be in the weak coupling limit, others in the intermediate coupling limit. On what follows we will give examples of both regimes in measurements that were carried out in three-terminal devices incorporating a thiol end-capped

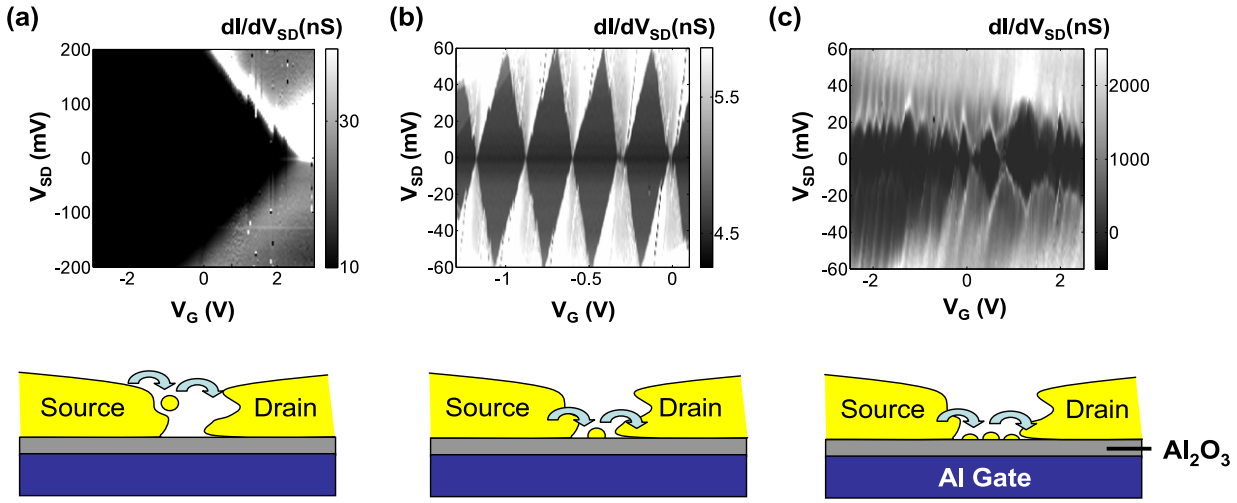

Figure 4.4. Stability diagrams and corresponding illustrations for three different cases. (a) Well-coupled island (very small gold grain or molecule) to the source electrode, but well shielded from the gate (low gate coupling): $\beta = 0.03$ and $\Gamma = 17.5$ meV. Electron transport through one (b) and several gold grains in series (c) lying on top of the gate dielectric (high gate coupling): $\beta = 0.27$, $\Gamma = 5.4$ meV in (b) and $\beta > 0.2$ in (c).

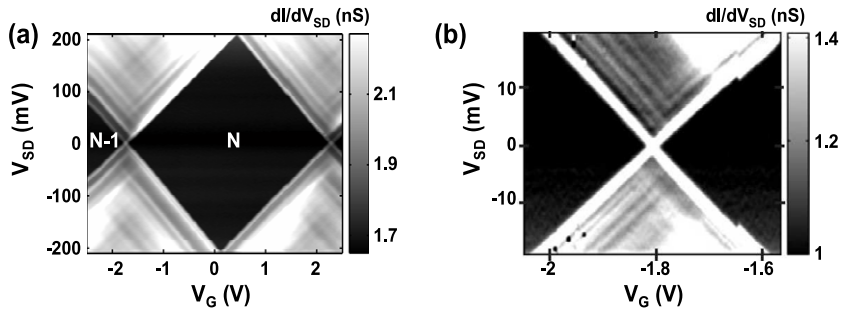

Figure 5.1. Stability diagrams of a three-terminal junction with OPV-5, in the weak coupling limit, measured at 1.6 K ($\beta = 0.05$, $\Gamma = 3$ meV). Three different charge states are probed. The $N + 1$ state is not indicated; for low bias voltages it starts at gate voltages larger than 2.2 V. The data yield an addition energy of 210 meV and a gate coupling of 0.05. (b) Zoom-in of the stability diagram shown in (a) near the degeneracy point separating the $N - 1$ from the N state.

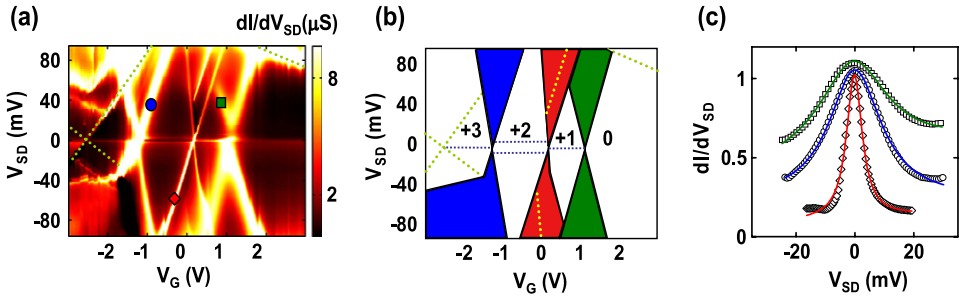

Figure 5.2. (a) Stability diagram of a three-terminal junction with OPV-5, measured at 1.7 K. Dotted green lines indicate the diamond edges of a second molecule connected in parallel. (b) Schematic drawing of the important information contained in (a) with the charge filling sequence as discussed in the text. (c) Differential conductance traces, $\mathrm{d}I/\mathrm{d}V_{\mathrm{SD}}$, along three different diamond edges at positions indicated in (a) (curves are normalized and then offset by 0.05 and centered at zero for clarity). Drawn lines represent fits to a Lorentzian peak shape with a lifetime broadening, Γ, that equals 6 meV (red), 22 meV (blue) and 35 meV (green).

oligophenylenevinylene molecules (OPV-n molecules) and $[\mathrm{Co}_4^{\mathrm{II}}\mathrm{L}_4]^{8+}[2 \times 2]$-grid type complexes [70].

5.1. Weak coupling (OPV-5): spectroscopy in the SET regime

OPV-5 consists of five benzene rings that are connected through double bonds [71]. The molecule has alkane side arms to make it soluble in common solvents. Figure 5.1 shows a stability diagram of a device incorporating such a molecule in which the molecule–lead coupling is low [10]. Typical current I levels for this device are hundreds of picoamps, indicating that subsequent tunneling processes are separated by 1 ns on average. It clearly shows the presence of sets of excitation lines for all three charge states accessible in the experiment. Further inspection reveals that the point of intersection between the lines and the diamond edge are symmetric with respect to the bias polarity, and that their position is almost independent of the charge state. Their appearance, on the other hand, may depend on the charge state, that is, an excitation may not be visible for all three charge states. At most, only a very weak variation (less than a few millielectronvolts) of the excitation energy with the charge state is present, and this observation makes it unlikely that the excitations are a result of electronic states, because these are expected to depend strongly on the charging of the molecule. Moreover, the 17 excitations present in the experimental data are unlikely to reflect precisely 17 available electronic states that differ by only 5–10 meV in energy, particularly for a small molecule that can only contain a limited number of electrons/holes. We therefore attribute the excitations to the vibrational modes of the single OPV-5 molecule trapped between the electrodes. We have also observed excitations at the same energies in other OPV-5 samples, although not all of them at the same time.

Figure 5.1(b) shows a zoom-in on the crossing point from $N - 1$ to N. For charge state N, excitations are present at 2.2, 3.5, 5.0 and 6.7 meV; for charge state $N - 1$ they appear at 2.4 and 3.7 meV. Again the values are symmetric with respect to the bias polarity. The energies do not form a harmonic spectrum since their values are not integer multiples of the 2.2 meV excitation and they may therefore be attributed to different vibrational modes. Within the error margins, however, the 6.7 meV excitation may be the second harmonic of the one at 3.5 meV, but no definite conclusion can be drawn from the measurements. Preliminary quantum-chemistry calculations, performed with the Amsterdam Density Functional program [72], indicate that there are a number of excitations in this energy range connected to the motion of the whole molecule attached to gold atoms on either side. More details about these modes will be published elsewhere.

5.2. Intermediate coupling (OPV-5)

An example of a measurement for the intermediate coupling case is presented in figure 5.2 [13]; numbers in figure 5.2(b) indicate the charge states (see the discussion below).

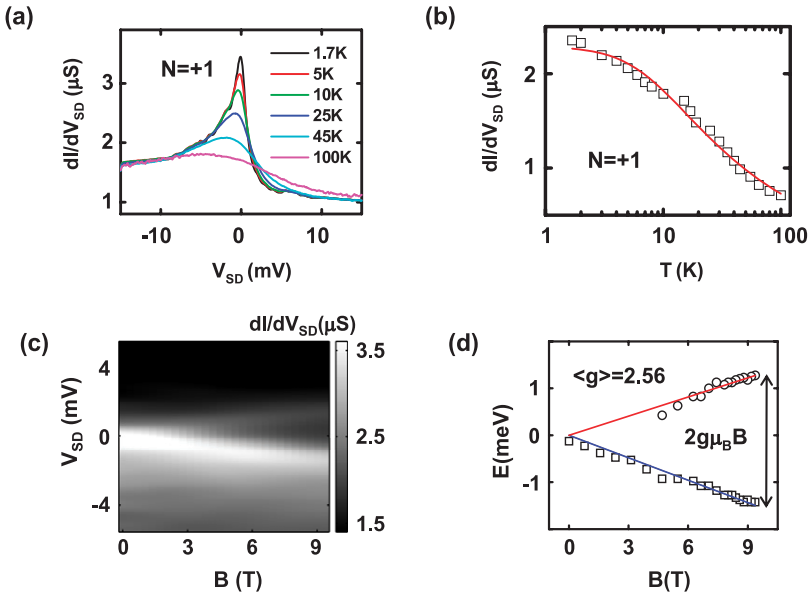

Figure 5.3. Kondo resonance characterization for $N = +1$ and $V_G = +0.56$ V. (a) dI/dV_{SD} versus V_{SD} for various temperatures. (b) Zero-bias conductance as a function of temperature. The red line is a fit to equation (1) with $s = 0.22$: the fitting parameters are $T_K = 37$ K, $G_c = 1.0\ \mu$S and $G_a = 2.3\ \mu$S. (c) Grayscale plot of dI/dV_{SD} versus V_{SD} and B. (d) Peak positions as a function of the magnetic field taken from the data in (c) indicating a g value of 2.56.

Cotunneling features are clearly visible in the low bias range as lines running parallel to the zero-bias axes. Zero-bias Kondo resonances are present in the $N = +1$ and $+3$ charge states; the $N = +2$ state reveals two finite-bias resonances located symmetrically around zero bias. The assignment of the charge-state occupancy has been carried out by magnetic-and temperature-dependent measurements of these low bias resonances. The temperature and magnetic field dependences of the Kondo resonance at $N = +1$ are shown in figure 5.3. The data are in good agreement with the theoretical expectations discussed in section 3.2. For $N = +3$ we have performed a similar analysis, which again is in good agreement with the characteristic features of the $S = 1/2$ Kondo effect.

Measurements on the finite-bias peaks inside the $N = +2$ diamond show that a magnetic field splits each peak into two clear peaks. At negative bias, the third derivative (figure 5.4(c)) indicates the presence of three peaks. This evolution in a magnetic field, B, is consistent with inelastic cotunneling from a singlet ground state to an excited triplet state (see figure 5.4(b)) [73, 74]. The splitting in each peak should be $g\mu_B m_s B$ with $m_s = \pm 1$. With a g factor of 2 the splitting in figure 5.4(c) yields an m_s value of 0.87 at negative bias and 1.0 at positive bias, consistent with the identification of the triplet state as the excited state. From the magnetic field measurements, we conclude [13] that the Coulomb diamond with the split peaks in zero magnetic field had a ground state with an even occupancy. We assigned $N = +2$ to this state, and starting from this, the electronic and spin spectrum was identified using a model that involves two weakly interacting states with an antiferromagnetic exchange energy J of 1.7 meV [13].

A closer inspection of the stability diagram reveals that the diamond edges are sharper for the $N = +2$ state compared

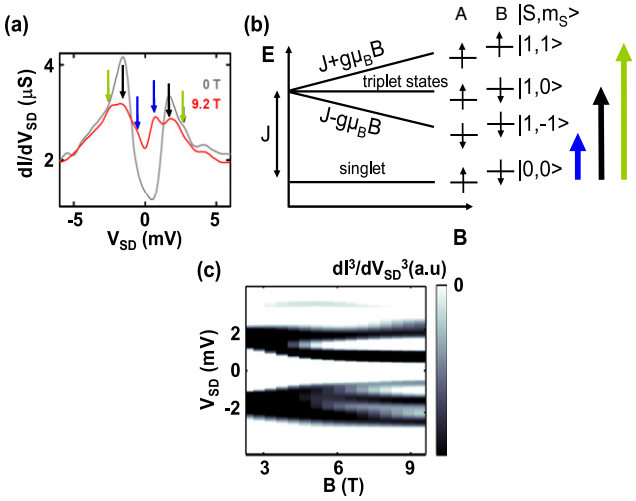

Figure 5.4. Characterization of the small bias inelastic cotunneling peaks for $N = +2$ and $V_G = -0.72$ V. (a) dI/dV_{SD} versus V_{SD} traces measured in a magnetic field of $B = 0$ T (gray) and $B = 9.2$ T (red). Arrows indicate the predicted positions of peaks at $B = 9.2$ T assuming a singlet ground state and a triplet excited state. In a magnetic field, the triplet splits by $g\mu_B B m_S$ with $g = 2$ and $m_S = -1, 0, 1$ as illustrated in (b). J is the antiferromagnetic exchange energy between states A and B. (c) Grayscale plot of d^3I/dV_{SD}^3 versus V_{SD} obtained by numerical differentiation of the measured dI/dV_{SD}. The third derivative underlines the presence of three (two) peaks for negative (positive) bias voltage.

to $N = +1$ and $+3$. For the region where electron tunneling involves $0 \rightarrow +1 \rightarrow 0$ transitions, a Lorentzian fit through the dI/dV_{SD} versus V_{SD} lineshape yields $\Gamma \approx 35$ meV; for the $+1 \rightarrow +2 \rightarrow +1$ and $+2 \rightarrow +3 \rightarrow +2$ transitions, $\Gamma \approx 6$ and 22 meV, respectively (figure 5.2(c)). A related observation

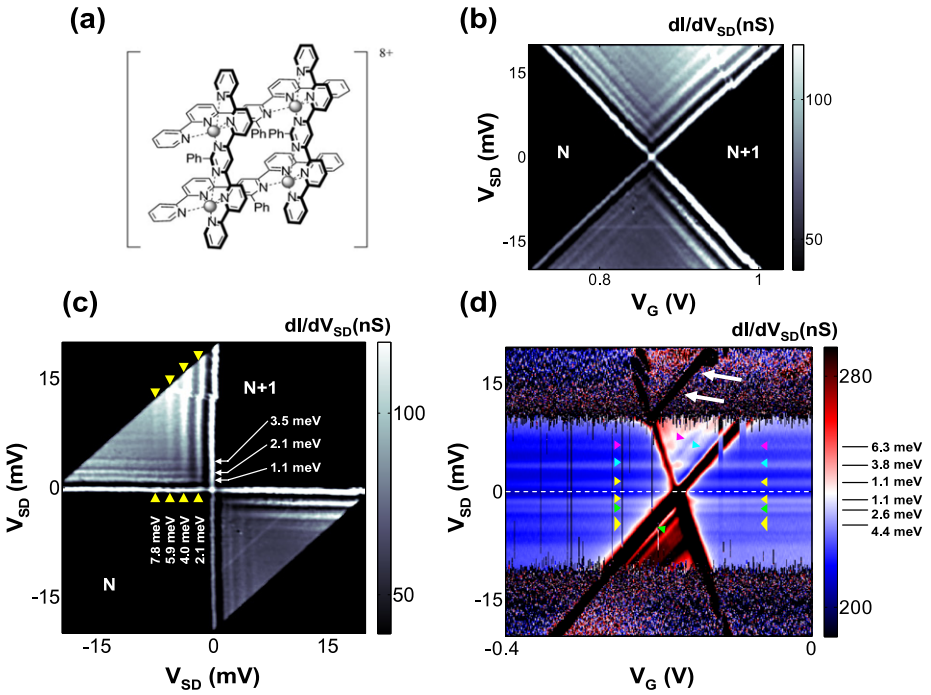

Figure 5.5. (a) Representation of the $[Co^{II}_4L_4]^{8+}$ complex (L = 4,6-bis(2,2′bipyrid-6-yl)-2-phenylpyrimidine). Each Co^{II} center is coordinated by six N donor atoms (dotted lines) [70]. (b) Stability diagram of a three-terminal junction incorporating a grid type complex in the weak coupling limit ($\beta = 0.07$, $\Gamma = 2$ meV), measured at 1.6 K. Two different charge states are probed. (c) Same as (b) but after a rotation and shearing transformation; the excitation energies are then read off directly on both orthogonal axes. Yellow arrows indicate a series of harmonic excitations. (d) Stability diagram of a different junction; intermediate coupling regime ($\beta = 0.09$, $\Gamma = 3$ meV). Arrows in the blocked region point at inelastic cotunneling excitations; white arrows point at an excitation in the SET regime. Yellow broad arrows (bottom) indicate a series of excitations that cannot be resolved individually due to thermal broadening. Cyan, purple and green arrows point at cotunneling excitations that match excitations in the SET region (i.e. they are connected to lines in the SET regime). The origin of the pronounced noise bands above $|V_{SD}| > 10$ meV is not yet understood.

is that the gate coupling for the three different charge states is not the same. For charge state +1, +2 and +3, β equals 0.06, 0.1 and 0.07, respectively. Thus, the $N = +2$ charge distribution on the molecule is more susceptible to the gate field. Apparently, the wavefunctions are located more to the middle of the junction in agreement with the lower electronic coupling for this charge state. For OPV-5 this dependence may be expected as discussed in detail in [13].

5.3. Grids (weak and intermediate coupling)

The $[Co^{II}_4L_4]^{8+}$[2 × 2]-grid type complex presented in figure 5.5(a) is a special type of molecule which gives rise to seven well-resolved reduction waves in cyclic voltammetry studies [70], i.e. seven electrons can be added to the molecule in solution. In figure 5.5 we show measurements carried out in electromigrated junctions which exemplify the two different coupling limits which we already encountered in the OPV-5 junctions. The stability plot in figure 5.5(b) shows sharp spectroscopic features in the SET region indicating a weak electronic coupling. Given the energy spacing of the excitations (a few meV) and their appearance at more or less the same energies for two subsequent charge states, we argue in the same way as above that the observed excitations originate from vibrational modes. Further confirmation comes from the observation of four harmonic excitation lines as shown in figure 5.5(c) by the yellow arrows. Such a harmonic spectrum indicates the excitation of four vibrational quanta and suggest a value of the electron–phonon coupling higher than one (see section 3).

Figure 5.5(d) shows the stability diagram of a different junction, which is an example of the intermediate electronic coupling case. In both charge states, inelastic cotunneling excitations are present at the same energies which indicate that these are due to vibrational excited states. The fact that three of these cotunneling lines match excitations inside the SET region makes it very unlikely that they are associated with a parallel conduction path (e.g. another molecule). The noise band at the top and bottom of the stability diagram and which starts—at positive bias—at the onset of conduction of an excited state (white arrows) is at present not understood. The intensity of the line at +10 meV is much higher than all others. Possibly, it is an electronic excitation. Note that in this case no Kondo features are present around zero bias.

5.4. Inelastic cotunneling through vibrational excited states in OPV-3 junctions

We have also carried out experiments with three-terminal devices incorporating a thiol end-capped oligophenylenevinylene molecule, in which three benzene rings are connected through two double bonds (OPV-3). The stability diagram presented in

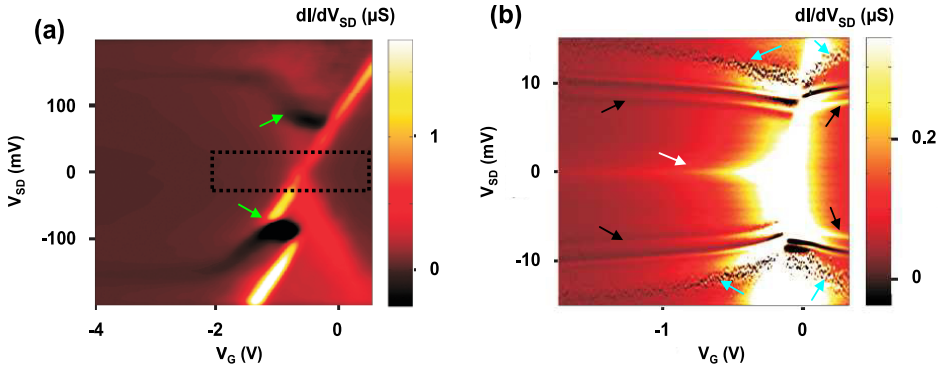

Figure 5.6. (a) Two-dimensional color plot of the differential conductance, $\mathrm{d}I/\mathrm{d}V_{\mathrm{SD}}$, versus V_{SD} and V_{G} at 1.7 K for a three-terminal device incorporating an OPV-3 molecule ($\beta = 0.07$, $\Gamma = 16$ meV). Green arrows point at two very pronounced negative differential resistance (NDR) regions. (b) Zoom-in inside the dashed black box in (a). Arrows point at a Kondo resonance (white), inelastic cotunneling (black) and intermittent noise (cyan).

figure 5.6(a) is for one of these junctions and it shows larger addition energies ($\geqslant$0.4 eV) than junctions with OPV-5, in agreement with recent measurements by Danilov *et al* [75]. Figure 5.6(b) is a high resolution scan for the small bias range around the degeneracy point. At zero bias, a Kondo resonance (white arrow) is clearly visible on the left side of the degeneracy point and absent on the right side, illustrating the parity effect discussed earlier. Additional lines (black arrows), symmetric in V_{SD}, are observed for both charge states bending towards the degeneracy point. The appearance of these inelastic cotunneling features at nearly the same energy for different charge states suggests that these excitations are likely to be vibrational rather than electronic. The evolution of the cotunneling features towards zero energy as the charge degeneracy point is approached is not fully understood at present. Similar observations have been reported by Natelson and coworkers [11]. Interestingly, over the whole gate voltage of the inelastic cotunneling excitations are followed by 'noise bands' (cyan arrows) symmetric in V_{SD} and present on both charge states. This could be further evidence that such excitations are vibrational. As pointed out by Galperin *et al* [54], strong electron–phonon coupling can give rise to intermittent noise in the junction current which could be a signature of multi-stable behavior; conformational fluctuations in the molecule could also lead to the observed noise.

6. Summary

We have reviewed different transport mechanisms for conduction through molecular junctions emphasizing the molecular signatures probed by three-terminal transport through single molecules. On the one hand these signatures are related to the coupling of electron transport to nuclear motion which leads to the observation of vibrational excitations. More subtle indications of conduction through single molecules involve changes in the electronic and gate couplings as a function of charge state resulting from a change in the spatial distribution of the charge. This observation raises an important question as to know where does the excess of charge localize along the molecular chain when it is brought in close contact to metallic leads, an issue that has not received much attention as of yet. Our measurements on OPV-5 seem to indicate localization of charges near the electrodes and for a doubly charged molecule this leads to an intrinsic double-dot-like configuration. In the ground state the spins of the charges are antiferromagnetically coupled with an exchange energy of 1.7 meV. In search of other signatures of molecular conduction, interesting candidates include conformational changes, which may lead to distinct negative differential resistance and hysteresis effects, and high-spin states as present in single-molecule magnets. In addition, contrary to inorganic semiconductors, molecules offer the possibility of controlling electronic properties at the atomic level by means of synthetic chemistry. Many surprises and new transport phenomena are still to be expected.

Acknowledgments

We thank Kevin O'Neill for the work on electromigration, Hubert Heersche and Zeger de Groot for the measurements on OPV-3, Jos Seldenthuis, Jos Thijssen and Jens Paaske for discussions. Financial support is obtained from the Dutch Organization for Fundamental Research on Matter (FOM), the 'Nederlandse Organisatie voor Wetenschappelijk Onderzoek' (NWO), the EU FP7 project SINGLE (contract no. 213609) and the 'Deutsche Forschungsgemeinschaft' (DFG) within the project 'Kondo Molecules'.

References

[1] Natelson D 2007 Single-molecule transistors *Handbook of Organic Electronics and Photonics* vol 3, ed H S Nalwa (Stevenson Ranch, CA: American Scientific Publishers) pp 1–49

[2] Nitzan A and Ratner M A 2003 Electron transport in molecular wire junctions *Science* **300** 1384–9

[3] Paulsson M and Stafstrom S 2001 Self-consistent-field study of conduction through conjugated molecules *Phys. Rev.* B **64** 035416

[4] Di Ventra M, Pantelides S T and Lang N D 2000 First-principles calculation of transport properties of a molecular device *Phys. Rev. Lett.* **84** 979

[5] Paulsson M, Zahid F and Datta S 2002 Resistance of a molecule *Preprint* cond-mat/0208183

[6] Qiu X H, Nazin G V and Ho W 2004 Vibronic states in single molecule electron transport *Phys. Rev. Lett.* **92** 206102

[7] Stipe B C, Rezaei M A and Ho W 1998 Single-molecule vibrational spectroscopy and microscopy *Science* **280** 1732

[8] Stipe B C, Rezaei M A and Ho W 1998 Coupling of vibrational excitation to the rotational motion of a single adsorbed molecule *Phys. Rev. Lett.* **81** 1263

[9] Gaudioso J, Lee H J and Ho W 1999 Vibrational analysis of single molecule chemistry: ethylene dehydrogenation on Ni(110) *J. Am. Chem. Soc.* **121** 8479

[10] Osorio E A, O'Neill K, Stuhr-Hansen N, Nielsen O F, Bjørnholm T and van der Zant H S J 2007 Addition energies and vibrational fine structure measured in electromigrated single-molecule junctions based on an oligophenylenevinylene derivative *Adv. Mater.* **19** 281–5

[11] Yu L H, Keane Z K, Ciszek J W, Cheng L, Stewart M P, Tour J M and Natelson D 2005 Inelastic electron tunneling via molecular vibrations in single-molecule transistors *Phys. Rev. Lett.* **95** 256803

[12] Park H, Park J, Lim A K L, Anderson E H, Alivisatos A P and McEuen P L 2000 Nanomechanical oscillations in a single-C_{60} transistor *Nature* **407** 57

[13] Osorio E A, O'Neill K, Wegewijs M, Stuhr-Hansen N, Paaske J, Bjørnholm T and van der Zant H S J 2007 Electronic excitations of a single molecule contacted in a three-terminal configuration *Nano Lett.* **7** 3336–42

[14] Heersche H B, de Groot Z, Folk J A and van der Zant H S J 2006 Electron transport through single Mn_{12} molecular magnets *Phys. Rev. Lett.* **96** 206801

[15] Jo M H, Grose J E, Baheti K, Deshmukh M M, Sokol J J, Rumberger E M, Hendrickson D N, Long J R, Park H and Ralph D C 2006 Signatures of molecular magnetism in single-molecule transport spectroscopy *Nano Lett.* **6** 2014

[16] Smit R H M, Noat Y, Untiedt C, Lang N D, van Hemert M C and van Ruitenbeek J M 2002 Measurement of the conductance of a hydrogen molecule *Nature* **419** 906

[17] Park H, Lim A K L, Alivisatos A P, Park J and McEuen P L 1999 Fabrication of metallic electrodes with nanometer separation by electromigration *Appl. Phys. Lett.* **75** 301

[18] Heersche H B, Lientschnig G, O'Neill K, van der Zant H S J and Zandbergen H W 2007 *In situ* imaging of electromigration-induced nanogap formation by transmission electron microscopy *Appl. Phys. Lett.* **91** 072107

[19] Taychatanapat T, Bolotin K I, Kuemmeth F and Ralph D C 2007 Imaging electromigration during the formation of break junctions *Nano Lett.* **7** 652

[20] Kubatkin S, Danilov A, Hjort M, Cornil J, Bredas J-L, Stuhr-Hansen N, Hedegard P and Bjornholm T 2003 Single-electron transistor of a single organic molecule with access to several redox states *Nature* **425** 698–701

[21] Kubatkin S, Danilov A, Hjort M, Cornil J, Bredas J L, Stuhr-Hansen N, Hedegård P and Bjørnholm T 2004 Single electron transistor with a single conjugated molecule *Curr. Appl. Phys.* **4** 554

[22] Champagne A R, Pasupathy A N and Ralph D C 2005 Mechanically adjustable and electrically gated single-molecule transistors *Nano Lett.* **5** 305

[23] Dadosh T, Gordin Y, Krahne R, Khivrich I, Mahalu D, Frydman V, Sperling J, Yacoby A and Bar-Joseph I 2005 Measurement of the conductance of single conjugated molecules *Nature* **436** 677

[24] Kouwenhoven L P, Marcus C M, Mceuen P L, Tarucha S, Westervelt R M and Wingreen N S 1997 Electron transport in quantum dots *Mesoscopic Electron Transport: Proc. NATO Advanced Study Institute (Curacao, June–July 1996)* (*Kluwer Series E345*) ed L L Sohn, L P Kouwenhoven and G Schö (Berlin: Springer) pp 105–214

[25] Likharev K K 1999 Single-electron devices and their applications *Proc. IEEE* **87** 606

[26] Glazman L I and Pustilnik M 2005 Low-temperature transport through a quantum dot *Nanophysics: Coherence and Transport* ed H Bouchiat *et al* (Amsterdam: Elsevier) pp 427–78

[27] Ono Y, Fujiwara A, Nishiguchi K, Inokawa H and Takahashi Y 2005 Manipulation and detection of single electrons for future information processing *J. Appl. Phys.* **97** 031101

[28] Averin D V and Nazarov Y V 1992 *Single Charge Tunneling: Coulomb Blockade Phenomena in Nanostructures* ed H Grabert and M H Devoret (New York: Plenum and NATO Scientific Affairs Division) p 217

[29] Marcus R A 1956 On the theory of oxidation–reduction reactions involving electron transfer *J. Chem. Phys.* **24** 966

[30] McConnell H M 1961 Intramolecular charge transfer in aromatic free radicals *J. Chem. Phys.* **35** 508

[31] Kouwenhoven L and Glazman L 2001 Revival of the Kondo effect *Phys. World* **14** 33–8

[32] Grobis M, Rau I G, Potok R M and Goldhaber-Gordon D 2007 Kondo effect in mesoscopic quantum dots *Handbook of Magnetism and Advanced Magnetic Materials* vol 5, ed H Kronmuller (New York: Wiley)

[33] Goldhaber-Gordon D, Shtrikman H, Mahalu D, Abusch-Magder D, Meirav U and Kastner M A 1998 Kondo effect in a single-electron transistor *Nature* **391** 156

[34] Goldhaber-Gordon D, Gores J, Kastner M A, Shtrikman H, Mahalu D and Meirav U 1998 From the Kondo regime to the mixed-valence regime in a single-electron transistor *Phys. Rev. Lett.* **81** 5225

[35] Houck A A, Labaziewwicz J, Chan E K, Folk J A and Chuang I L 2005 Kondo effect in electromigrated gold break junctions *Nano Lett.* **5** 1685–8

[36] Park J, Pasupathy A N, Goldsmith J I, Chang C, Yaish Y, Petta J R, Rinkoski M, Sethna J P, Abruña H D, McEuen P L and Ralph D C 2002 Coulomb blockade and the Kondo effect in single-atom transistors *Nature* **417** 722

[37] Yu L H, Keane Z K, Ciszek J W, Cheng L, Tour J M, Baruah T, Pederson M R and Natelson D 2005 Kondo resonances and anomalous gate dependence in the electrical conductivity of single-molecule transistors *Phys. Rev. Lett.* **95** 256803

[38] Liang W, Shores M P, Bockrath M, Long J R and Park H 2002 Kondo resonance in a single-molecule transistor *Nature* **417** 725

[39] Yu L H and Natelson D 2004 The Kondo effect in C_{60} Single-molecule transistors *Nano Lett.* **4** 79

[40] Kondo J 1964 Resistance minimum in dilute magnetic alloys *Prog. Theor. Phys.* **32** 37

[41] Pustilnik M and Glazman L 2004 Kondo effect in quantum dots *J. Phys.: Condens. Matter* **16** R513–37

[42] Anderson P W 1961 Localized magnetic states in metals *Phys. Rev.* **124** 41

[43] Glazman L I and Raikh M E 1988 Resonant Kondo transparency of a barrier with quasilocal impurity states *JETP Lett.* **47** 452

[44] Costi T A, Hewson A C and Zlatic V 1994 Transport coefficients of the Anderson model via the numerical renormalization group *J. Phys.: Condens. Matter* **6** 2519

[45] Pustilnik M, Glazman L I, Cobden D H and Kouwenhoven L P 2000 Magnetic field-induced Kondo effects in Coulomb blockade systems *Preprint* cond-mat/0010336

[46] Buitelaar M R, Bachtold A, Nussbaumer T, Iqbal M and Schönenberger C 2002 Multiwall carbon nanotubes as quantum dots *Phys. Rev. Lett.* **88** 156801

[47] Nygård J, Cobden D H and Lindelof P E 2000 Kondo physics in carbon nanotubes *Nature* **408** 342

[48] van der Wiel W G, De Franceschi S, Fujisawa T, Elzerman J M, Tarucha S and Kouwenhoven L P 2000 The Kondo effect in the unitary limit *Science* **289** 2105
[49] Jarillo-Herrero P, Kong J, van der Zant H S J, Dekker C, Kouwenhoven L P and De Franceschi S 2005 Orbital Kondo effect in carbon nanotubes *Nature* **434** 484
[50] Sasaki S, De Franceschi S, Elzerman J M, van der Wiel W G, Eto M, Tarucha S and Kouwenhoven L P 2000 Kondo effect in an integer-spin quantum dot *Nature* **405** 764
[51] Pustilnik M, Avishai Y and Kikoin K 2000 Quantum dots with even number of electrons: Kondo effect in a finite magnetic field *Phys. Rev. Lett.* **84** 1756
[52] Eto M and Nazarov Y V 2000 Enhancement of Kondo effect in quantum dots with an even number of electrons *Phys. Rev. Lett.* **85** 1306
[53] De Franceschi S, Sasaki S, Elzerman J M, van der Wiel W G, Tarucha S and Kouwenhoven L P 2001 Electron cotunneling in a semiconductor quantum dot *Phys. Rev. Lett.* **86** 878
[54] Galperin M, Ratner M A and Nitzan A 2007 Molecular transport junctions: vibrational effects *J. Phys.: Condens. Matter* **19** 103201
[55] Troisi A and Ratner M A 2006 Molecular signatures in the transport properties of molecular wire junctions: what makes a junction 'molecular' ? *Small* **2** 172
[56] Gaudioso J, Lauhon L J and Ho W 2000 Vibrationally mediated negative differential resistance in a single molecule *Phys. Rev. Lett.* **85** 1918
[57] Wingreen N S, Jacobsen K W and Wilkins J W 1988 Resonant tunneling with electron–phonon interaction: an exactly solvable model *Phys. Rev. Lett.* **61** 1396
[58] Mitra A, Aleiner I and Millis A J 2004 Phonon effects in molecular transistors: quantal and classical treatment *Phys. Rev.* B **69** 245302
[59] Braig S and Flensberg K 2003 Vibrational sidebands and dissipative tunneling in molecular transistors *Phys. Rev.* B **68** 205324
[60] Koch J and von Oppen F 2005 Franck–Condon blockade and giant Fano factors in transport through single molecules *Phys. Rev. Lett.* **94** 206804
[61] Wegewijs M R and Nowack K C 2005 Nuclear wavefunction interference in single-molecule electron transport *New J. Phys.* **7** 239
[62] Boese D and Schoeller H 2001 Influence of nanomechanical properties on single-electron tunneling: a vibrating single-electron transistor *Europhys. Lett.* **54** 668
[63] Schatz G C and Ratner M A 2002 *Quantum Mechanics in Chemistry* (Mineola, NY: Dover)
[64] O'Neill K, Osorio E A and van der Zant H S J 2007 Self-breaking in planar few-atom Au constrictions for nanometer-spaced electrodes *Appl. Phys. Lett.* **90** 133109
[65] Tsutsui M, Shoji K, Taniguchi M and Kawai T 2008 Formation and self-breaking mechanism of stable atom-sized junctions *Nano Lett.* **8** 345
[66] Strachan D R, Smith D E, Johnston T H, Therien M J, Bonnell D A and Johnson A T 2005 Controlled fabrication of nanogaps in ambient environment for molecular electronics *Appl. Phys. Lett.* **86** 043109
[67] Lörtscher E, Ciszek J W, Tour J and Riel H 2006 Reversible and controllable switching of a single-molecule junction *Small* **2** 973
[68] Esen G and Fuhrer M S 2005 Temperature control of electromigration to form gold nanogap junctions *Appl. Phys. Lett.* **87** 263101
[69] Gonzalez J I, Lee T H, Barnes M D, Antoku Y and Dickson R M 2004 Quantum mechanical single-gold-nanocluster electroluminescent light source at room temperature *Phys. Rev. Lett.* **93** 147402
[70] Ruben M, Breuning E, Barboiu M, Gisselbrecht J P and Lehn J M 2003 Functional supramolecular devices: $[M^{II}_4L_4]^{+8}[2 \times 2]$-grid type complexes as multilevel molecular electronic species *Chem. Eur. J.* **9** 291
[71] Stuhr-Hansen N, Christensen J B, Harrit N and Bjørnholm T 2003 Novel synthesis of protected thiol end-capped stilbenes and oligo(phenylenevinylene)s (OPVs) *J. Org. Chem.* **68** 1275
[72] Velde G, Bickelhaupt F M, Baerends E J, Guerra C F, van Gisbergen S J A, Snijders J G and Ziegler T J 2001 Chemistry with ADF *Comput. Chem.* **22** 931
[73] Paaske J, Rosch A, Wölfle P, Mason N, Marcus C M and Nygård J 2006 Non-equilibrium singlet–triplet Kondo effect in carbon nanotubes *Nat. Phys.* **2** 460
[74] Kogan A, Granger G, Kastner M A and Goldhaber-Gordon D 2003 Singlet–triplet transition in a single-electron transistor at zero magnetic field. *Phys. Rev.* B **67** 113309
[75] Danilov A, Kubatkin S, Kafanov S, Hedegård P, Stuhr-Hansen N, Moth-Poulsen K and Bjørnholm T 2008 Electronic transport in single molecule junctions: control of the molecule–electrode coupling through intramolecular tunneling barriers *Nano Lett.* **8** 1–5